IN-02
61460
P-42

NASA Contractor Report 4419

On the Wall-Normal Velocity of the Compressible Boundary-Layer Equations

C. David Pruett

CONTRACT NAS1-18599
DECEMBER 1991

NASA Contractor Report 4419

On the Wall-Normal Velocity of the Compressible Boundary-Layer Equations

C. David Pruett
Analytical Services & Materials, Inc.
Hampton, Virginia

Prepared for
Langley Research Center
under Contract NAS1-18599

National Aeronautics and
Space Administration
Office of Management
Scientific and Technical
Information Program
1991

ON THE WALL-NORMAL VELOCITY OF THE COMPRESSIBLE BOUNDARY-LAYER EQUATIONS

C. David Pruett†

Analytical Services and Materials, Inc.
107 Research Drive
Hampton, Virginia 23666

SUMMARY

We consider a problem which arises in the numerical solution of the compressible two-dimensional or axisymmetric boundary-layer equations. Numerical methods for the compressible boundary-layer equations are facilitated by transformation from the physical (x,y) plane to a computational (ξ,η) plane in which the evolution of the flow is "slow" in the time-like ξ direction. The commonly used Levy-Lees transformation results in a computationally well-behaved problem, but it complicates interpretation of the solution in physical space. Specifically, the transformation is inherently nonlinear, and the physical wall-normal velocity is transformed out of the problem and is not readily recovered. Conventional methods extract the wall-normal velocity in physical space from the continuity equation, using finite-difference techniques and interpolation procedures. The present spectrally-accurate method extracts the wall-normal velocity directly from the transformation itself, without interpolation, leaving the continuity equation free as a check on the quality of the solution. The present method for recovering wall-normal velocity, when used in conjunction with a highly-accurate spectral collocation method for solving the compressible boundary-layer equations, results in a discrete solution which satisfies the continuity equation nearly to machine precision. As demonstration of the utility of the method, the boundary layers of three prototypical high-speed flows are investigated and compared: the flat plate; the hollow cylinder; and the cone. An important implication for classical linear stability theory is also briefly discussed.

† This work was conducted partially during the author's period of tenure as a National Research Council Associate at NASA Langley Research Center. Completion of the work was accomplished under NASA Contract NAS1-18599, Task C-3, by the Theoretical Flow Physics Branch, Fluid Mechanics Division, NASA Langley Research Center, with Analytical Services and Materials, Inc.

1. INTRODUCTION

In modern aerodynamics, the boundary-layer approximation is an invaluable tool of widespread applicability. Although it is still beyond the capability of existing supercomputers to solve the compressible Navier-Stokes equations for complete aerodynamic configurations, it is commonplace for engineering purposes to patch inviscid "outer" solutions to the Euler equations with "inner" solutions to the boundary-layer equations to obtain realistic lift and drag estimates. A different application, and the motivation for this work, lies in the area of stability and transition, for which solutions to the boundary-layer equations provide the mean velocity and temperature distributions necessary for linear and nonlinear stability analyses. In this latter context, accuracy is quite important, since, in general, the stability of wall-bounded flow is extremely sensitive to variations in the mean.

The boundary-layer equations define an initial-boundary-value-problem (IBVP) in which the streamwise spatial coordinate is time-like. The solution is obtained by streamwise marching procedures. The equations are extraordinarily "stiff", particularly for high-speed compressible flow. Consequently, only implicit marching techniques have met with practical success (for example, see the finite-difference method of Harris and Blanchard [1], or the spectral collocation method of Pruett and Streett [2]). Depending on the geometry of the flow, the time-like derivative may either enhance or undermine the diagonal dominance of the Jacobian used in the iteration procedure. To facilitate the numerical solution it is customary to transform the boundary-layer equations from physical (x,y) space to a computational (ξ,η) space in which the time-like derivative has "nice" properties. In the ideal situation, a similarity solution exists, and the time-like derivative vanishes identically with the proper similarity transformation. Similarity solutions exist, however, only for a limited class of flows (e.g.; flow over a flat plate in the absence of a streamwise pressure gradient). For non-similar flows, it is desirable that the time-like evolution in the transform plane be "slow", and that the time-like derivative contribute to diagonal dominance of the Jacobian.

One transformation which exhibits these traits for a wide class of boundary-layer flows is that known commonly as the Levy-Lees transformation [3]*. Although the Levy-Lees transformation results in a computationally well-behaved problem, it complicates interpretation of the results in physical

space, relative to the more straightforward transformations used for specialized applications by Duck [4], and by Pruett and Streett [2]. First, it is inherently nonlinear, an additional reason why fully-implicit methods are necessary. Second, the physical v-velocity is transformed out of the computational problem and is not easily recovered. For some applications, this is not of major concern. For example, classical linear stability analyses, which invoke the parallel-flow approximation, disregard the wall-normal velocity. It is now recognized, however, that the non-parallel effects on the stability of a high-speed flow can be significant [5], and methods are being adapted and developed to treat non-parallelism. Among these are spatial direct numerical simulation (SDNS) [6], multiple scales analyses (MS) [7,8], and a recent scheme based on the parabolized stability equations (PSE) [9,10]. Each requires accurate determination of wall-normal velocity, and the MS and PSE methods require its gradient as well. The quality (smoothness) of the solution is of particular importance whenever the application requires differentiated velocities.

Conventional methods exploit finite-difference techniques and obtain the wall-normal velocity from the continuity equation (J. E. Harris, private communication). The method presented here, designed as a companion to the spectral collocation method for the compressible boundary-layer equations (CBLE) developed by Pruett and Streett [2], enjoys two major advantages over conventional approaches. First, the wall-normal velocity is computed to spectral accuracy. Second, the wall-normal velocity is extracted directly from the coordinate transformation, leaving the continuity equation available as a check on the quality of the solution. Using the method of [2] for the CBLE, and the present method to extract wall-normal velocity, we obtain a discrete solution which satisfies the continuity equation nearly to machine precision. Moreover, we obtain second derivatives of temperature and velocity distributions which are smooth to at least seven decimal places.

At the heart of the present method lies the non-trivial evaluation of the quantity η_x. In the next section the governing equations and non-dimensionalization are discussed, and the Levy-Lees transformation is presented. The third section details the numerical method, focusing on two independent

*White [3], however, refers to this as the Illingworth-Levy-Lees-Dorodnitsyn-Probstein-Elliot transformation, mentioning also the contribution of Mangler.

derivations for η_x, both of which lead to complicated expressions. In the fourth section, in which we validate the method, both derivations of η_x are shown to give virtually identical numerical results. The fifth section provides an application of the method whereby the high-speed boundary layers of a flat plate, a hollow cylinder, and a sharp cone are compared, with particular attention to their respective wall-normal velocity distributions. An important implication regarding the linear stability of the flow along a cone is also discussed. Finally, brief concluding remarks are offered in the last section.

2. GOVERNING EQUATIONS

We consider the laminar boundary-layer flow along a two-dimensional or axisymmetric body at zero angle of incidence. In regions of the flow in which the boundary-layer approximation is valid, the flow is governed by [1]

$$\frac{\partial}{\partial x}(r^j \rho u) + \frac{\partial}{\partial \bar{y}}(r^j \rho \bar{v}) = 0 \tag{1a}$$

$$\rho u \frac{\partial u}{\partial x} + \rho \bar{v} \frac{\partial u}{\partial \bar{y}} = -\frac{\partial p}{\partial x} + \frac{1}{r^j} \frac{\partial}{\partial \bar{y}} \left[r^j \mu \frac{\partial u}{\partial \bar{y}} \right] \tag{1b}$$

$$\rho u \frac{\partial T}{\partial x} + \rho \bar{v} \frac{\partial T}{\partial \bar{y}} = u \frac{\partial p}{\partial x} + \frac{1}{r^j \cdot Pr} \frac{\partial}{\partial \bar{y}} \left[r^j \kappa \frac{\partial T}{\partial \bar{y}} \right] + \mu \left[\frac{\partial u}{\partial \bar{y}} \right]^2 \tag{1c}$$

$$p = \frac{(\gamma - 1)}{\gamma} \rho T \tag{1d}$$

$$\bar{y} = \sqrt{Re}\, y \quad ; \quad \bar{v} = \sqrt{Re}\, v \tag{1e}$$

Dimensionless equations (1a,b,c) are derived from the compressible Navier-Stokes equations via the boundary-layer approximation [3], and describe, respectively, conservation of mass, streamwise momentum, and energy. Equation (1d) is the equation of state, and Eq. (1e) defines a convenient scaling. Here, we assume the fluid to be an ideal gas. For j=0 and j=1, Eqs. (1) describe, respectively, two-dimensional and axisymmetric boundary-layer flow.

In Eqs. (1), x is the arc length along the body measured from the stagnation point, y is the wall-

normal coordinate, and $r = r_0 + y\cos\phi$ is the radial coordinate from the axis of revolution, as shown in Fig. 1. In general, $r_0 = r_0(x)$ and $\phi = \phi(x)$. Two axisymmetric bodies of particular interest here are the cone and the hollow cylinder, the latter of which is the axisymmetric analog of the flat plate. For the cone, ϕ is the (fixed) cone half-angle, and $r_0(x) = x\sin\phi$. For the hollow cylinder, r_0 is the (fixed) radius, and $\phi = 0$.

In Eqs. (1), u and v denote dimensionless velocity components in the x and y dimensions, respectively. The remaining dimensionless variables T, ρ, μ, and κ are, respectively, the temperature, density, viscosity, and thermal conductivity. Lengths are normalized by an arbitrary reference length L^*, and flow quantities are normalized as follows:

$$u = \frac{u^*}{u_r^*} \quad ; \quad v = \frac{v^*}{u_r^*} \quad ; \quad \rho = \frac{\rho^*}{\rho_r^*} \quad ; \tag{2}$$

$$T = \frac{T^*}{T_r^*} \quad ; \quad p = \frac{p^*}{\rho_r^* u_r^{*2}} \quad ; \quad \mu = \frac{\mu^*}{\mu_r^*} \quad ; \quad \kappa = \frac{\kappa^*}{\kappa_r^*}$$

Throughout this paper, dimensional quantities are denoted by an asterisk. In Eqs. (2), the reference velocity u_r^* and the reference density ρ_r^* are arbitrary, and the reference temperature, viscosity, and thermal conductivity are defined as

$$T_r^* = \frac{u_r^{*2}}{C_p^*} \quad ; \quad \mu_r^* = \mu^*(T_r^*) \quad ; \quad \kappa_r^* = \kappa^*(T_r^*) \tag{3}$$

Governing equations (1) are closed by assuming $\mu(T)$ and $\kappa(T)$ to vary according to the Sutherland law; namely,

$$\mu = \kappa = \frac{T^{3/2}(1+C_1)}{T+C_1} \quad ; \quad C_1 = \frac{198.6\ ^\circ R}{T_e^*} \tag{4}$$

The dimensionless parameters which arise as a result of the scalings in Eq. (2) are the Mach number M, Reynolds number Re, the Prandtl number Pr, and the ratio of specific heats γ. Specifically, these are defined as

$$M = \frac{u_r^*}{a_r^*} \quad ; \quad Re = \frac{\rho_r^* u_r^* L^*}{\mu_r^*} \quad ; \quad Pr = \frac{C_p^* \mu_r^*}{\kappa_r^*} \quad ; \quad \gamma = \frac{C_p^*}{C_v^*} \tag{5}$$

where $a_r^* = \sqrt{\gamma R_g^* T_r^*}$ is the reference speed of sound, R_g^* is the ideal gas constant, and C_p^* and C_v^* are, respectively, the specific heats at constant pressure and constant volume. For ideal gases, C_p^* and C_v^* are constant, and $R_g^* = C_p^* - C_v^*$.

The Levy-Lees transformation [3], commonly used to facilitate the numerical solution of Eqs. (1), has the following form:

$$\xi(x) = \int_0^x \rho_e u_e \mu_e r_0^{2j} dx \tag{6a}$$

$$\eta(x,y) = \frac{\sqrt{Re}\,\rho_e u_e r_0^j}{\sqrt{2\xi}} \int_0^y t^j \frac{\rho}{\rho_e} dy \tag{6b}$$

$$t = \left[\frac{r}{r_0}\right]^j = \begin{cases} 1 & (j=0) \\ 1 + \dfrac{y\cos\phi}{r_0} & (j=1) \end{cases} \tag{6c}$$

In Eqs. (6) and subsequent discussion, subscript "e" denotes edge values, which, in general, depend on x. With the further transformations

$$F = \frac{u}{u_e} \quad ; \quad \theta = \frac{T}{T_e} \tag{7a}$$

$$V = \frac{2\xi}{\rho_e u_e \mu_e r_0^{2j}} \left[F \frac{\partial \eta}{\partial x} + \frac{\rho \bar{v} r^j}{\sqrt{2\xi}} \right] \tag{7b}$$

governing Eqs. (1) take the following form in the transform plane [1]:

$$\frac{\partial V}{\partial \eta} + 2\xi \frac{\partial F}{\partial \xi} + F = 0$$

$$2\xi F \frac{\partial F}{\partial \xi} + V \frac{\partial F}{\partial \eta} - \frac{\partial}{\partial \eta}\left[t^{2j} \frac{\mu}{\theta} \frac{\partial F}{\partial \eta} \right] + \frac{2\xi}{u_e} \frac{du_e}{d\xi} (F^2 - \theta) = 0 \tag{8}$$

$$2\xi F \frac{\partial \theta}{\partial \xi} + V \frac{\partial \theta}{\partial \eta} - \frac{\partial}{\partial \eta}\left[t^{2j} \frac{\mu}{\theta} \frac{\partial \theta}{\partial \eta} \right] - (\gamma - 1) M_e^2 t^{2j} \frac{\mu}{\theta} \left[\frac{\partial F}{\partial \eta} \right]^2 = 0$$

We note that transformed governing equations (8) make use of

$$\frac{\rho}{\rho_e} = \frac{1}{\theta} \tag{9}$$

which is obtained from the equation of state (1d) and the boundary-layer approximation $\frac{\partial p}{\partial y} \cong 0$.

In the experience of the author, transformation (6) is essential for the accurate numerical solution of a non-similar boundary-layer flow in which the streamwise velocity profile becomes "thinner" as one proceeds downstream; e.g., boundary-layer flow along a sharp cone. For example, when the spectral collocation method of Pruett and Streett [2] using the straightforward transformation of Duck [4] is applied for the case of M_e=6.8 flow over a 7° half-angle cone, the Jacobian of the iteration procedure becomes very ill-conditioned. For a highly-resolved grid the condition number can be $O(10^{15})$ or larger. In contrast, when transformation (6) is incorporated into the method, the condition number for a highly-resolved grid is typically $O(10^8)$. In the former case, the extreme ill-conditioning prevents full convergence of the iteration procedure, resulting in an excessively noisy solution.

3. NUMERICAL METHODS

From Eqs. (7b) and (9) one obtains the following expression for the wall-normal velocity v in the transform (ξ,η) plane:

$$v(\xi,\eta) = \frac{\sqrt{2\xi}}{\sqrt{Re}} \frac{\theta}{r^j} \left[\frac{u_e \mu_e r_0^{2j} V}{2\xi} - \frac{F}{\rho_e} \frac{\partial \eta}{\partial x} \right] \tag{10}$$

Provided the quantities on the right hand side of Eq. (10) are known, the determination of v is trivial. The difficulty with Eq. (10), however, is that a closed-form expression for η_x is not readily available, nor is its form simple. Because of the complicated nature of η_x, we present two independent derivations which we then use for (numerical) cross-validation. In the first method, η_x is obtained from the Jacobians of transformation (6) and its inverse. In the second method, η_x is shown to be the solution of a linear Fredholm integral equation whose coefficients are constructed from information available from the solution of Eqs. (8). For both methods, the computational effort required to evaluate η_x (and subsequently v) is insignificant relative to that required to solve boundary-layer Eqs. (8).

Before proceeding, we note that the evaluation of t in the boundary-layer Eqs. (8), and both methods for evaluating η_x, make use of the inverse transformation corresponding to Eqs. (6). Whereas the inverse of (6a) is straightforward and is omitted, the inverse of (6b) requires the solution of a quadratic equation which results in the following numerically-stable form:

$$y(\xi,\eta) = \begin{cases} \dfrac{\sqrt{2\xi}}{\sqrt{Re}\,\rho_e u_e}\displaystyle\int_0^{\eta}\theta d\eta \equiv y_{2D} & (j=0) \\ \dfrac{2y_{2D}}{r_0(1+\sqrt{1+C})} & (j=1) \end{cases} \tag{11a}$$

where

$$C(\xi,\eta) \equiv \frac{2\cos\phi\, y_{2D}}{r_0^2} \tag{11b}$$

Note that the planar (j=0) expression must be evaluated to obtain y_{2D} prior to evaluation of the axisymmetric (j=1) expression.

Method 1

From Eqs. (6) we obtain

$$\frac{\partial \xi}{\partial x} = \frac{d\xi}{dx} = \left[\frac{dx}{d\xi}\right]^{-1} \tag{12a}$$

$$\frac{\partial \eta}{\partial y} = \left[\frac{\partial y}{\partial \eta}\right]^{-1} \tag{12b}$$

$$\frac{\partial \eta}{\partial x} = -\frac{\partial \eta}{\partial y}\frac{\partial y}{\partial \xi}\frac{d\xi}{dx} \tag{12c}$$

To derive Eqs. (12) we have made use of the fact that the product of the Jacobians of transformation (6) and its inverse must yield the 2×2 identity matrix. Two of the factors necessary to evaluate (12c) are easily obtained from Eqs. (6). They are

$$\frac{d\xi}{dx} = \rho_e u_e \mu_e r_0^{2j} \tag{13a}$$

$$\frac{\partial y}{\partial \eta} = \frac{\sqrt{2\xi}\theta}{\sqrt{Re}\,\rho_e u_e r^j} \tag{13b}$$

The remaining factor y_ξ is complicated. After straightforward though tedious differentiation of Eq. (11) with respect to ξ, we obtain

$$\frac{\partial y}{\partial \xi}(\xi,\eta) = \begin{cases} \left[\frac{1}{2\xi} - \frac{1}{\rho_e}\frac{d\rho_e}{d\xi} - \frac{1}{u_e}\frac{du_e}{d\xi}\right] y_{2D} + \frac{\sqrt{2\xi}}{\sqrt{Re}\,\rho_e u_e}\int_0^\eta \frac{\partial \theta}{\partial \xi} d\eta \equiv \frac{\partial y_{2D}}{\partial \xi} & (j=0) \\ \left[\frac{1}{r_0}\frac{dr_0}{d\xi} + \tan\phi\frac{d\phi}{d\xi}\right] y - \frac{1}{r_0}\left[\frac{2}{r_0}\frac{dr_0}{d\xi} + \tan\phi\frac{d\phi}{d\xi}\right]\frac{y_{2D}}{\sqrt{1+C}} + \frac{1}{r_0\sqrt{1+C}}\frac{\partial y_{2D}}{\partial \xi} & (j=1) \end{cases} \tag{14}$$

We note that Leibnitz' Rule has been exploited for differentiation beneath the integral sign in Eq. (11a). As in the case of Eq. (11), one must evaluate the planar (j=0) expression prior to the axisymmetric (j=1) expression. The wall-normal velocity v follows immediately from Eqs. (14), (12c), and (10).

Derivatives of the edge and geometry data $\tau(\xi) \in (\rho_e, u_e, \mu_e, r_0, \phi)$ are evaluated by the chain rule as follows:

$$\frac{d\tau}{d\xi} = \frac{d\tau}{dx}\left(\frac{d\xi}{dx}\right)^{-1} \tag{15}$$

where $\frac{d\xi}{dx}$ is given in Eq. (13a). We defer discussion of the procedure for numerically evaluating the integral expressions in Eqs. (11) and (14) until after the the presentation of Method 2.

Method 2

First, some mathematical preliminaries are in order. In the steps to follow, we exploit the chain rule

$$\frac{\partial\theta}{\partial x} = \frac{\partial\theta}{\partial\xi}\frac{d\xi}{dx} + \frac{\partial\theta}{\partial\eta}\frac{\partial\eta}{\partial x} \tag{16}$$

and the integral transformation

$$\int_0^y h(y)dy = \int_0^\eta h(\eta)\frac{\partial y}{\partial\eta}d\eta \tag{17}$$

where h is an arbitrary function of (ξ,η) with ξ fixed, and where $\frac{\partial y}{\partial\eta}$ is given in Eq. (13b).

Differentiating transformation (6b) with respect to x, we obtain

$$\frac{\partial\eta}{\partial x}(x,y) = \frac{\eta}{\rho_e}\frac{d\rho_e}{dx} + \frac{\eta}{u_e}\frac{du_e}{dx} + j\left[\frac{\eta}{r_0}\frac{dr_0}{dx}\right] - \frac{\eta}{2\xi}\frac{d\xi}{dx} + \frac{\sqrt{Re}\,\rho_e u_e r_0 \dot{}}{\sqrt{2\xi}}\frac{\partial}{\partial x}\int_0^y \frac{t}{\theta}dy \tag{18}$$

By applying Leibnitz' Rule to differentiate under the integral sign, and by invoking the product rule, we obtain

$$\frac{\partial}{\partial x}\int_0^y \frac{t}{\theta}dy = \int_0^y\left[\frac{1}{\theta}\frac{\partial t}{\partial x} - \frac{t}{\theta^2}\frac{\partial\theta}{\partial x}\right]dy = \int_0^y \frac{1}{\theta}\frac{\partial t}{\partial x}dy - \int_0^y \frac{t}{\theta^2}\frac{\partial\theta}{\partial x}dy \tag{19}$$

From definition (6c) and some algebraic manipulation, the following expression for $\frac{\partial t}{\partial x}$ results:

$$\frac{\partial t}{\partial x} = j\left[\tan\phi\frac{d\phi}{dx} + \frac{1}{r_0}\frac{dr_0}{dx}\right](1-t) \tag{20}$$

Expanding the first integral expression on the right hand side of Eq. (19) using Eqs. (17) and (20), we

obtain the following expression in terms of (ξ,η):

$$\int_0^y \frac{1}{\theta}\frac{\partial t}{\partial x}dy = j\frac{\sqrt{2\xi}}{\sqrt{Re}\,\rho_e u_e r_0^j}\left[\tan\phi\frac{d\phi}{dx} + \frac{1}{r_0}\frac{dr_0}{dx}\right]\left[-\eta + \int_0^\eta \frac{1}{t}d\eta\right] \tag{21}$$

Similarly, the second integral expression on the right hand side of Eq. (19) is derived to be

$$\int_0^y \frac{t}{\theta^2}\frac{\partial\theta}{\partial x}dy = \frac{\sqrt{2\xi}}{\sqrt{Re}\,\rho_e u_e r_0^j}\left[\frac{d\xi}{dx}\int_0^\eta \frac{1}{\theta}\frac{\partial\theta}{\partial\xi}d\eta + \int_0^\eta \frac{1}{\theta}\frac{\partial\theta}{\partial\eta}\frac{\partial\eta}{\partial x}d\eta\right] \tag{22}$$

where chain rule (16) has been invoked for $\frac{\partial\theta}{\partial x}$.

The desired integral form is obtained by combining Eqs. (18-22), whereby

$$\begin{aligned}\frac{\partial\eta}{\partial x}(\xi,\eta) = &\left[\frac{1}{\rho_e}\frac{d\rho_e}{dx} + \frac{1}{u_e}\frac{du_e}{dx} - \frac{1}{2\xi}\frac{d\xi}{dx} - j\tan\phi\frac{d\phi}{dx}\right]\eta \\ &+ j\left[\tan\phi\frac{d\phi}{dx} + \frac{1}{r_0}\frac{dr_0}{dx}\right]\int_0^\eta \frac{1}{t}d\eta - \frac{d\xi}{dx}\int_0^\eta \frac{1}{\theta}\frac{\partial\theta}{\partial\xi}d\eta - \int_0^\eta \frac{1}{\theta}\frac{\partial\theta}{\partial\eta}\frac{\partial\eta}{\partial x}d\eta\end{aligned} \tag{23}$$

We note that certain terms containing $\frac{1}{r_0}\frac{dr_0}{dx}$ have exactly canceled in the derivation of Eq. (23).

Expression (23) is a linear Fredholm integral equation of the form

$$q(\xi,\eta) = \int_0^\eta w(\xi,\eta)q(\xi,\eta)d\eta + p(\xi,\eta) \tag{24a}$$

where

$$q(\xi,\eta) = \frac{\partial\eta}{\partial x} \tag{24b}$$

$$w(\xi,\eta) = \frac{-1}{\theta}\frac{\partial\theta}{\partial\eta} \tag{24c}$$

$$p(\xi,\eta) = f(\xi)\eta + g(\xi)d(\xi,\eta) - e(\xi,\eta) \tag{24d}$$

and where

$$f(\xi) \equiv \frac{1}{\rho_e}\frac{d\rho_e}{dx} + \frac{1}{u_e}\frac{du_e}{dx} - \frac{1}{2\xi}\frac{d\xi}{dx} - j\tan\phi\frac{d\phi}{dx} \tag{24e}$$

$$g(\xi) \equiv j\left[\tan\phi\frac{d\phi}{dx} + \frac{1}{r_0}\frac{dr_0}{dx}\right] \tag{24f}$$

$$d(\xi,\eta) \equiv \int_0^\eta \frac{1}{t}d\eta \tag{24g}$$

$$e(\xi,\eta) \equiv \frac{d\xi}{dx}\int_0^\eta \frac{1}{\theta}\frac{\partial\theta}{\partial\xi}d\eta \tag{24h}$$

We relegate the details of the discretization of Eq. (24a) to the Appendix. We note, however, that Eq. (24a) is linear and its matrix analog is Nth-order; consequently, the computational effort necessary to extract v is insignificant relative to that of solving Eqs. (8), which require the iterative solution of systems of order $3M$.

In practice, whether by Method 1 or Method 2, evaluation of η_x occurs along contours of constant ξ. For ξ fixed, the integrals which appear in both methods (for example; in Eqs. (13) and (24)) assume the form

$$i(\eta) \equiv \int_0^\eta h(\eta)d\eta \tag{25}$$

where h is again an arbitrary function of η. It remains to describe their spectrally-accurate numerical approximation. For this purpose, let the computational domain $0 \le \eta \le \eta_{MAX}$ be partitioned into N subintervals such that $0=\eta_0<\eta_1<\eta_2<\cdots<\eta_N=\eta_{MAX}$. At the grid points η_n we have

$$i(\eta_n) = \sum_{k=0}^{n}\Delta i(\eta_k) \quad ; \quad \Delta i(\eta_n) \equiv \begin{cases} 0 & (n=0) \\ \int_{\eta_{n-1}}^{\eta_n} h(\eta)d\eta & (n=1,2,\ldots,N) \end{cases} \tag{26}$$

If $h_n \equiv h(\eta_n)$, and i_n and Δi_n are the discrete approximations of $i(\eta_n)$ and $\Delta i(\eta_n)$, respectively, then the

discrete analog of Eq. (26) is the following:

$$i_n = \sum_{k=0}^{n} \Delta i_k \quad ; \quad \vec{\Delta i}_1 = \mathbf{Q}\,\vec{h} \tag{27}$$

In Eq. (27) $\mathbf{Q}$ is an $N\times(N+1)$ quadrature operator, and, for convenience, the following vector notation is adopted:

$$\vec{h} \equiv \begin{bmatrix} h_0 \\ h_1 \\ \cdot \\ \cdot \\ \cdot \\ h_N \end{bmatrix} \quad ; \quad \vec{h}_1 \equiv \begin{bmatrix} h_1 \\ h_2 \\ \cdot \\ \cdot \\ \cdot \\ h_N \end{bmatrix} \tag{28}$$

Conventions similar to Eqs. (28) hold for all other vector quantities.

Eq. (27) is general in the sense that $\mathbf{Q}$ can represent any quadrature rule. For example, if the trapezoidal quadrature rule is adopted, then $\mathbf{Q}$ is bidiagonal and $\vec{i}$ approximates $i(\eta)$ to second-order accuracy. For the hydrodynamic stability applications which motivate this work, we are interested in attaining highly accurate and smooth solutions. Accordingly, we specialize $\mathbf{Q}$ to a collocation method based on Chebyshev polynomial approximation, for which $\mathbf{Q}$ is a dense matrix and for which spectral accuracy is attained. The collocation method applied here to the extraction of the wall-normal velocity is described in [2], to which the reader is referred for greater detail. For completeness, we summarize briefly below.

Let continuous non-periodic function $h(\mathfrak{h})$ on [-1,1] be approximated by a finite series expansion $h_N(\mathfrak{h})$ in an orthogonal basis set of Chebyshev polynomials $T_n(\mathfrak{h})$, namely

$$h_N(\mathfrak{h}) = \sum_{n=0}^{N} \hat{h}_n T_n(\mathfrak{h}) \tag{29a}$$

$$T_n(\mathfrak{h}) = \cos\left[n \cos^{-1}\mathfrak{h}\right] \tag{29b}$$

where coefficients $\hat{h}_n$ are termed the "spectrum" of $h_N(\mathfrak{h})$. Using the "natural" Gauss-Lobatto set of

collocation points

$$\eta_n = \cos z_n \quad ; \quad z_n = \frac{\pi n}{N} \quad ; \quad (n = 0,1,2,...,N) \tag{30}$$

we obtain from Eq. (29) the discrete Fourier cosine transform

$$h_n \equiv h_N(\eta_n) = \sum_{k=0}^{N} \hat{h}_k \cos\frac{n\pi k}{N} \tag{31}$$

The corresponding discrete inverse transform gives the spectrum $\hat{h}_n$, namely

$$\hat{h}_n = \frac{2}{Nc_n} \sum_{k=0}^{N} \frac{h_k}{c_k} \cos\frac{n\pi k}{N} \tag{32a}$$

where

$$c_k = \begin{cases} 2 & k=0 \text{ or } k=N \\ 1 & 0 < k < N \end{cases} \tag{32b}$$

It is convenient to express Eq. (32) as a matrix-vector operation

$$\vec{\hat{h}} = \mathbf{P}_N \vec{h} \tag{33}$$

where $\mathbf{P}_N$ is a dense $(N+1)\times(N+1)$ matrix whose elements are available by inspection from Eqs. (32).

Interpreted in the light of transform pair (31) and (32), Eqs. (29) define the spectral interpolation polynomial, exact, by definition, at the collocation points. Unlike polynomial interpolating series defined on equally spaced intervals, series (29) converges uniformly to $h(\eta)$ as $N \to \infty$. Moreover, it can be shown that, for continuously differentiable functions h, coefficients $\hat{h}_n$ decay to zero faster than any finite power of $1/N$ as $N \to \infty$. This is termed "spectral convergence".

Now, to form quadrature operator $\mathbf{Q}$ we consider

$$\int_{\eta_{n-1}}^{\eta_n} h(\eta)d\eta \cong E_n \equiv \int_{\eta_{n-1}}^{\eta_n} h_N(\eta)d\eta = \int_{\eta_{n-1}}^{\eta_n} \sum_{k=0}^{N} \hat{h}_k T_k(\eta)d\eta = \sum_{k=0}^{N} \hat{h}_k \int_{\eta_{n-1}}^{\eta_n} T_k(\eta)d\eta \tag{34}$$

In matrix-vector form, Eq. (34) becomes

$$\vec{E}_1 = \mathbf{R}_N \vec{h} \tag{35}$$

where $\vec{E}_1$ is an N-vector and $\mathbf{R}_N$ is a dense $N\times(N+1)$ matrix whose elements are obtained from Eq. (34) with the help of Eqs. (29) and (30) as follows:

$$R_{kn} = -\int_{z_{k-1}}^{z_k} \sin z \cos(kz)\,dz \qquad \begin{matrix}(k = 1,2,\ldots,N)\\(n = 0,1,2,\ldots,N)\end{matrix} \tag{36}$$

From Eqs. (33) and (35) the $N\times(N+1)$ spectral quadrature operator $\mathbf{Q}$ is defined as

$$\mathbf{Q} = \mathbf{R}_N \mathbf{P}_N \tag{37}$$

We note that a continuous mapping $\eta=\eta(\tilde{\eta})$ is necessary to take the natural Chebyshev domain $-1\le\tilde{\eta}\le1$ onto the computational domain $0\le\eta\le\eta_{MAX}$. Such a mapping is also useful to redistribute collocation points, clustering them in regions of high gradients. In practice, the metric $\frac{d\tilde{\eta}}{d\eta}$, computed either analytically, or numerically to spectral accuracy, is incorporated directly into quadrature operator $\mathbf{Q}$. Finally, we note that $\mathbf{Q}$ should be computed initially in double-precision arithmetic to avoid catastrophic loss of significance, The double-precision representation is subsequently truncated to single precision for numerical quadrature via Eq. (27). Since $\mathbf{Q}$ is computed but once, the additional computational effort is minimal.

We close by summarizing briefly the complete algorithm for extracting wall-normal velocity, as integrated into the spectral collocation boundary-layer algorithm of Pruett and Streett [2]. Following [2], governing equations (8) are solved for discrete marching steps $\xi_0<\xi_1<\xi_2<\cdots$, each corresponding to a unique streamwise station. Immediately available from the converged boundary-layer solution at each fixed ξ are the quantities θ, θ_ξ, θ_η, and t which appear in the integrands of Eqs. (11a), (14), and (24). These integrals are evaluated numerically to spectral accuracy following the quadrature procedure of Eqs. (27-37). In the discrete approximation, the integral expressions are vector quantities. Also needed at each discrete ξ are certain scalar quantities: for example; $f(\xi)$ and $g(\xi)$ in Eqs. (24) of

Method 2, or the coefficient of y_{2D} in Eq. (14) of Method 1. These are readily evaluated from the discrete edge and geometry data $\tau[\xi(x)]$. Currently, we use cubic splines for smooth interpolation of τ as well as for computation of derivatives of the form $d\tau/dx$. Following the evaluation of all necessary scalar and vector quantities at fixed ξ, the discrete approximation of η_x is obtained either from Eqs. (12-14) in Method 1, or from integral equation (24) in Method 2. Wall-normal velocity is obtained subsequently from Eq. (10) and the boundary-layer solution (V,F,θ). Despite the awkward nature of the expressions which comprise Methods 1 and 2, their evaluations are straightforward, are computationally efficient, and involve only the numerical machinery already in place for the solution of boundary-layer equations (8).

4. CODE VALIDATION

Our purpose here is to offer reasonable validation of the present method. To obtain the results of this section, we solve Eqs. (8) by the fully-implicit method of Pruett and Streett [2], which has been modified to incorporate the Levy-Lees transformation (6). We exploit second-order backward differencing in the time-like dimension, although the method allows up to 5th-order differencing. For convenience, the marching scheme uses equally-spaced steps in physical space. A further modification permits the option of either preconditioned Richardson iteration or Newton iteration within each implicit marching step. Typically, we iterate using the Richardson scheme until the discrete residual is small enough so that one final (computationally-intensive) Newton iteration achieves "full" convergence. Following convergence of the iteration, the wall-normal velocity is extracted by the spectral collocation method presented herein. All computations assume that the wall is adiabatic, although the boundary-layer code permits fixed temperature wall conditions as well. The results shown below were obtained using 102 (N=101) collocation points in the wall-normal η direction, and constant increments of $\Delta x^* = 0.1$ ft. in the marching direction. The following transformation has been used to map from the Chebyshev domain $\bar{\eta} \in [-1,1]$ to the computational domain $\eta \in [0,\eta_{MAX}]$, as discussed in the previous section.

$$\eta(\bar{\eta}) = \frac{0.5\eta_{MAX}\left[1-\tanh(\sigma)\right](1-\bar{\eta})}{1-\tanh\left[0.5\sigma(1-\bar{\eta})\right]} \tag{38}$$

In Eq. (38), σ is a free parameter which controls the strength of stretching. The results shown use η_{MAX}=21 and σ=0.7, chosen after some numerical experimentation. For a well-resolved grid, the solution is not particularly sensitive to the choice of σ. However, it is important that η_{MAX} be sufficiently large that the far-field boundary condition does not "pinch" the boundary-layer flow. Our experience is that η_{MAX} should be chosen so that $y^*(\eta_{MAX})$ is 2 to 3 boundary-layer displacement thicknesses from the wall. We note that 102 collocation points are far more than the 40 or so necessary to obtain 3-digit "engineering" accuracy. In fact, as will be shown, at this resolution velocity and temperature distributions at fixed ξ are smooth to 13 digits.

We take the flow parameters and the geometry of the validation case from the high-speed (M_∞=8.0) wind-tunnel experiment of Stetson *et al* on a sharp cone at zero angle of incidence [11]. These are:

$$\phi = 7^\circ \quad ; \quad M_e = 6.8 \quad ; \quad T_e^* = 128^\circ \text{ R} \quad ; \quad Re_1 = 1.4\overline{3}\times 10^6 \text{ ft}^{-1} \tag{39}$$

where Re_1 is the unit Reynolds number based on edge conditions. Except quite near the tip, the flow on a sharp cone exhibits conditions at the boundary-layer edge which are approximately constant. Accordingly, we assume that the edge values remain constant in x, and we set reference values equal to their respective edge values; e.g., $u_r^*=u_e^*$. We note, however, that both methods for extracting v have been validated for the fully general case in which both the geometry and edge data vary with x.

Figure 2 compares the radial velocity obtained by the present method with the results of a parabolized Navier-Stokes (PNS) calculation using the well-tested code of Korte [12]. The PNS code exploits finite-difference techniques and is of second-order accuracy in both the marching (axial) s and cross-stream (radial) r directions. The velocities (u',v') computed by the PNS code are in cartesian coordinates, and for comparison, the results of the boundary-layer calculation are transformed accordingly. The PNS scheme is fully explicit and the marching step size is the maximum allowed by stability (CFL) considerations. The PNS computation uses 150 grid points in the radial dimension, approximately 30 of which lie within the boundary layer. At this resolution, the PNS calculation is fairly severely under-resolved in the radial direction as indicated by the clearly visible grid-scale oscillation.

In fact, as can be inferred from Harris [1], approximately 200 points are necessary to fully resolve the boundary layer region to engineering (3-digit) accuracy using 2nd-order finite difference methods. Unfortunately, it is impractical for existing computer resources to pack significantly more points within the boundary layer since, in the fully explicit PNS code, the marching step size decreases as Δr_{MIN}^{-2}, where Δr_{MIN} is the minimum grid interval in the radial dimension. Similar computational barriers were encountered when attempting to compare the present method against a compressible Navier-Stokes (NS) calculation using the finite-volume code of Jacobs [13], for which it was impractical to resolve the flow to the degree desired. Despite these difficulties, the radial velocities obtained from the PNS and boundary-layer (BL) computations, which are compared at s=3.28 ft. (1 meter) in Fig. 2, are in reasonable agreement. The maximum velocity, the boundary-layer edge location, and the far-field decay of v' all agree well. We note also that the shock obliqueness angle derived by the PNS calculation is about 11°, for which the corresponding post-shock Mach number is 6.8, in concurrence with the experimental results of Stetson *et al* and the edge Mach number used for the BL calculation. We further mention that the (under-resolved) NS [13] and PNS [12] calculations are in close agreement.

The present method has been further validated by Kopriva (in unpublished work), who has employed the spectral-collocation BL code to check recent adaptations of his spectral multidomain code (inviscid) [14] to incorporate the viscous terms of the CNSE. Agreement between Kopriva's moderately-resolved NS computations and the present method is quite good for test cases which include Mach 2 flow over a circular cylinder and Mach 2.2 flow over a flat plate.

The previous checks against existing codes assure us that there are no grievous errors in the current method of extracting wall-normal velocity. We turn now to self-consistency checks. One motivation for developing independent methods for evaluating η_x is to provide a check otherwise unavailable. For the same test case as before, with parameter values given in Eqs. (39), Fig. 3 compares η_x at x^*=2.0 ft. as computed by Methods 1 and 2. These results appear virtually identical in Fig. 3, and, in fact, they agree to at least 11 significant digits at every gridpoint.

As mentioned in the introduction, the current method also leaves the continuity equation available as a check on the quality of the discrete solution. For later use, it is preferable to expand continuity

Eq. (1a), whereby we obtain the following expression, which is valid for flat-plate, hollow cylinder, and cone geometry:

$$\frac{\partial(\rho u)}{\partial x} + \frac{\partial(\rho v)}{\partial y} + j\frac{\rho u \sin\phi}{r} + j\frac{\rho v \cos\phi}{r} = 0 \tag{40}$$

Figure 4 presents the discrete residual of Eq. (40) at x^*=3.0 ft. along the cone, computed by summing the four terms on the left hand side. Again, the parameter values are those given in Eqs. (39). Derivatives are evaluated in computational space by the appropriate chain rules, thereby avoiding interpolation in physical space. The continuity equation is satisfied to approximately 11 orders of magnitude. That there remains considerable structure in the wall-normal distribution of the residuals suggests that, with further tuning of σ and N, one could likely drive the residual at least another order of magnitude toward machine zero (10^{-14}).

One final measure of the quality of the spectral numerical method is the decay of the spectra (refer to Eq. 32a) as shown at station x^*=3.0 ft. along the cone in Fig. 5. The decay of the temperature, u-velocity, and v-velocity spectra each by at least 13 orders of magnitude implies that the solution is smooth to nearly the full 14-digit precision of the (Cray 2) machine. The linear decay rate on the logarithmic scale is indicative of "spectral convergence", by which we mean that truncation error decays faster than any finite power of $1/N$ as $N \to \infty$.

Our interest in an accurate and smooth solution is not just academic. Analyses of stability based on parallel linear stability theory result in eigenvalue problems which require first and second partial derivatives with respect to y of both the mean u-velocity and the mean temperature. In addition, analyses based on non-parallel theory require the mean v-velocity and its derivatives as well. For N=101, each spectrally-accurate numerical differentiation of the boundary-layer solution results in a loss of significance of 2-3 digits due to the unavoidable magnification of round-off errors. Yet because of the initially high quality of the solution, we obtain first and second derivatives which are smooth to at least 10 and 7 digits, respectively.

Finally, we comment briefly on computational efficiency. For N=101, the spectral collocation method of Pruett and Streett [2] modified for the Levy-Lees transformation (6) requires slightly less

than one CPU-second per marching step on a Cray 2 supercomputer to solve boundary-layer equations (8). Of this second, extraction of the wall-normal velocity by Method 2 consumes a small percentage, whereas the computational requirements of Method 1 are virtually negligible. It was originally thought that the integral equation method (Method 2) might enjoy some advantages in the distribution of error. However, from the data for Fig. 3, it appears that any such advantage is insignificant.

5. APPLICATION

We turn now to an application of the method to a problem of both longstanding and immediate interest which concerns the stability characteristics of the boundary layers of cylinders and cones relative to those of the more commonly studied flat plate. While it is beyond the scope of this paper to address stability theory *per se*, some light is shed on stability issues by comparing boundary-layer "profiles" for the flat plate, the hollow cylinder, and the cone.

Here we consider the same flow parameters and cone geometry given in Eqs. (39). Presented for comparison, the hollow cylinder can be regarded as the axisymmetric equivalent of the flat plate (that is, the boundary layer is assumed to have no thickness at the sharp leading edge). The radius of the cylinder is taken to be r_0^*=0.3684 ft., equivalent to that of the cone at station x^*=3.0 ft. For reference, Fig. 6 compares the growth of the three boundary layers in terms of displacement thickness δ^* as defined below [3]:

$$\delta^*\left[1+\frac{\delta^*}{2r_0^*}\right]^j = \int_0^\infty \left[\frac{r^*}{r_0^*}\right]^j \left[1-\frac{\rho^* u^*}{\rho_e^* u_e^*}\right] dy^* \tag{41}$$

As is well known, the self-similar boundary layer on the flat plate grows proportionately to $\sqrt{x^*}$. On the other hand, the boundary layer along the cylinder is non-similar because the "curvature" K, quantified by the ratio $K=\delta^*/r_0^*$, increases in the streamwise direction due to the growth of δ^*. Provided $K \ll 1$, as is the case here, the displacement thickness on the cylinder exhibits growth much like that of the flat plate. Also as is well known, the boundary layer on the cone asymptotes to a growth rate $1/\sqrt{3}$ times that of the flat plate, as predicted by the Mangler transformation [15]. Mangler's theory

ignores transverse curvature and is invalid near the sharp tip of the cone where K is large. As noted by Malik and Spall [16], the curvature K along the cone *decreases* in the streamwise direction, in contrast to its increase along the cylinder. As they also note, the effect on stability of the disparity in scales is that the boundary layer on the cone supports higher disturbance frequencies.

Figures 7a-c compare, respectively, the temperature, streamwise velocity, and wall-normal velocity distributions of the cone, cylinder, and flat-plate boundary layers at x^*=3.0 ft. When the wall-normal coordinate y^* is scaled by the appropriate displacement thickness, the temperature and streamwise velocity distributions of the flat plate, hollow cylinder, and cone "collapse" and are virtually coincident. There is a slight effect due to transverse curvature which tends to produce a slightly "fuller" u-velocity profile and a "thinner" temperature profile with increasing K. For the parameter values of the test case, the curvature K values at x^*=3.0 ft. are 0.0, 0.0744, and 0.0440, for the flat plate, cylinder, and cone, respectively. Our principle interest lies in comparison of the wall-normal velocities. Whereas the v-velocity in the flat-plate boundary layer is constant at the edge, that of the cylinder decays like $1/r$ in the far field. Otherwise, they are qualitatively similar. In contrast to the hollow cylinder and flat plate, the cone has v-velocity which changes sign, is negative for large y, and has a large, nearly constant gradient in the far field. For comparison Fig. 7c also shows the inviscid solution for the wall-normal velocity, obtained from the code of Marconi and co-workers [17]. Note that the far-field boundary-layer solution and the inviscid solution have similar trends as anticipated, lending additional confidence in the method.

To highlight the influence of the differences in wall-normal velocity which are due to geometry, it is useful to examine the individual contributions of each of the four terms on the left hand side of continuity equation (40), as shown in Figs. 8. For the flat plate (Fig. 8a), the third and fourth terms vanish, and the first and second terms exactly balance. For the the cylinder (Fig. 8b) there is a small non-zero contribution from the fourth term, but the overall picture closely resembles that of the flat plate. In contrast, for the cone (Fig. 8c), terms 1 and 2 approximately balance in the near-wall region. However, the third term contains a large contribution in the far field which is offset approximately by the far-field contribution of the second term.

Figure 8c has implications for classical linear stability theory, in which the parallel-flow approximation plays an important role. In theory, the parallel-flow approximation arises from the recognition that the wall-layer mean flow evolves slowly in x relative to the scale of a typical disturbance wavelength, in which case certain terms in the linearized disturbance equations are "small" and can reasonably be neglected. In practice (i.e., in stability codes), however, the parallel-flow approximation is typically implemented by requiring of the mean flow that

$$v = 0 \qquad \text{and} \qquad \frac{\partial}{\partial x} = 0 \tag{42}$$

Condition (42) is self-consistent for the boundary-layer flow along a flat plate or a hollow cylinder in the sense that a parallel mean flow can simultaneously satisfy continuity Eq. (40) and approximation (42). From Fig. 8c, however, we find that Eqs. (40) and (42) are inconsistent for the cone, since the term $\rho u \sin\phi / r$ does not vanish under approximation (42). Violation of the continuity equation by the assumption of parallelism is particularly noxious since it leads to inconsistency between the conservative and nonconservative formulations of the linearized disturbance equations [18]. In fact, Pruett, Ng, and Erlebacher [18] have shown rigorously that there is no self-consistent parallel-flow approximation for the stability of the flow along a cone. If the stability of a conical flow is properly treated only by methods which allow non-parallelism, then the wall-normal velocity assumes importance. Consequently, the care which has been devoted here to securing an accurate and smooth determination of v is not ill spent.

6. CONCLUSIONS

The fully implicit, spectral collocation method developed by Pruett and Streett [2] for solution of the compressible boundary-layer equations has been extended to incorporate the Levy-Lees [3] transformation and spectrally-accurate evaluation of the wall-normal velocity. The Levy-Lees transformation is essential to the stability of the numerical method for certain classes of compressible boundary-layer flows; however, it renders determination of the wall-normal (v) velocity non-trivial. Two methods of determining v are presented and are shown to be numerically equivalent. The generalized algorithm is

valid for non-similar, two-dimensional or axisymmetric boundary-layer flow with varying edge conditions. Computation on a highly resolved mesh results in a discrete solution which satisfies the continuity equation nearly to machine precision, while requiring only about one second of CPU time per marching step on a Cray 2 supercomputer. Because of its generality, and the accuracy and smoothness of the discrete solution, the present method is well suited to providing the mean-flow velocity and temperature distributions needed for analyses of the stability of compressible boundary-layer flows, whether by classical linear stability theory or by recent methods which treat non-parallelism of the mean flow. Since mean-flow non-parallelism can significantly affect the stability of high-speed, wall-bounded flows [5], the contribution of wall-normal velocity should not be cavalierly disregarded.

ACKNOWLEDGEMENTS

The author is indebted to Drs. Julius Harris, Craig Streett, and C.-L. Chang for many helpful discussions and considerable insight. The assistance of Drs. John Korte, Peter Jacobs, and David Kopriva in validating results is also gratefully acknowledged.

APPENDIX

For completeness, we describe briefly a solution procedure for the discrete analog of integral Eq. (24a). For fixed ξ, Eq. (24a) has the form

$$q(\eta) = \int_0^{\eta} w(\eta) q(\eta) d\eta + p(\eta) \tag{A1}$$

Note, by inspection of Eqs. (24), $q(0) = 0$. From (A1) we obtain

$$q(\eta_n) - q(\eta_{n-1}) = \int_{\eta_{n-1}}^{\eta_n} w(\eta) q(\eta) d\eta + (p_n - p_{n-1}) \quad (n = 1,2,3,...,N) \tag{A2}$$

Following the notations regarding Eqs. (26-28), the discrete approximation of Eq. (A2) is

$$\mathbf{M}\vec{q}_1 = \mathbf{Q}_1 \mathbf{W}\vec{q}_1 + \Delta\vec{p}_1 \tag{A3}$$

where $\mathbf{W}$ is the $N \times N$ diagonal "weighting" matrix

$$\mathbf{W} = \begin{bmatrix} w_1 & & & \\ & w_2 & & \\ & & \ddots & \\ & & & w_N \end{bmatrix} , \tag{A4}$$

and $\mathbf{M}$ is the $N \times N$ bidiagonal matrix

$$\mathbf{M} = \begin{bmatrix} 1 & & & \\ -1 & 1 & & \\ & -1 & 1 & \\ & & \ddots & \ddots \\ & & & -1 \quad 1 \end{bmatrix} , \tag{A5}$$

$\mathbf{Q}_1$ is the $N \times N$ matrix formed by eliminating the first column of the $N \times (N+1)$ numerical quadrature operator $\mathbf{Q}$ (refer to Eq. 37), and $\Delta\vec{p}_1$ is the N-vector whose components are $\Delta p_n = p_n - p_{n-1}$ $(n = 1,2,3,...,N)$. Simplifying (A3), we obtain $\vec{q}_1$ as the solution to the Nth-order

linear system

$$\mathbf{A}\,\vec{q}_1 = \Delta\vec{p}_1 \qquad \text{where} \qquad \mathbf{A} \equiv \mathbf{M} - \mathbf{Q}_1\mathbf{W} \tag{A6}$$

REFERENCES

1) Harris, J. E., and D. K. Blanchard, "Computer Program for Solving Laminar, Transitional, or Turbulent Compressible Boundary-Layer Equations for Two-Dimensional and Axisymmetric Flow", *NASA TM-83207* (1982).

2) Pruett, C. D. and C. L. Streett, "A Spectral Collocation Method for Compressible, Nonsimilar Boundary Layers", *Int. J. Num. Meth. Fluids*, Vol. 13, No. 6, 713-737 (1991).

3) White, F. M., *Viscous Fluid Flow*, McGraw-Hill, New York (1974).

4) Duck, P. W., "The Inviscid Axisymmetric Stability of the Supersonic Flow Along a Cylinder", *ICASE Report 89-19 (NASA CR-181816)* (1989).

5) El-Hady, N. M., "Nonparallel Instability of Supersonic and Hypersonic Boundary Layers", *AIAA Paper No. 91-0324*, presented at the 29th Aerospace Sciences Meeting, Reno, Nevada, Jan. 7-10, 1991.

6) Thumm, A., W. Wolz, and H. Fasel, "Numerical Simulation of Spatially Growing Three-Dimensional Disturbance Waves in Compressible Boundary Layers", in *Laminar-Turbulent Transition: IUTAM Symposium, Toulouse, France, 1989*, eds. D. Arnal and R. Michel, Springer-Verlag, Berlin, 303-308 (1990).

7) El-Hady, N. M., "Spatial Three-Dimensional Secondary Instability of Compressible Boundary-Layer Flows", *AIAA J.*, Vol. 29, No. 5, 688-696 (1991).

8) Balakumar, P., and M. R. Malik, "Waves Produced from a Harmonic Point Source in a Supersonic Boundary Layer", *AIAA Paper No. 91-1646* (1991).

9) Bertolotti, F. P., *Linear and Nonlinear Stability of Boundary Layers with Streamwise Varying Properties*, PhD Thesis, Ohio State University (1990).

10) Chang, C.-L., M. R. Malik, G. Erlebacher, and M. Y. Hussaini, "Compressible Stability of Growing Boundary Layers using Parabolized Stability Equations", *AIAA Paper No. 91-1636* (1991).

11) Stetson, K. F., E. R. Thompson, J. C. Donaldson, and L. G. Siler, "Laminar Boundary-Layer Sta-

bility Experiments on a Cone at Mach 8. Part 1: Sharp Cone", *AIAA Paper No. 83-1761* (1983).

12) Korte, J. J., "An Explicit Upwind Algorithm for Solving the Parabolized Navier-Stokes Equations", *NASA TP-3050* (1991).

13) Jacobs, P. A., "Single-Block Navier-Stokes Integrator", *ICASE Interim Report 18 (NASA Contractor Report 187613)* (1991).

14) Kopriva, D. A., "Multidomain Spectral Solutions of High-Speed Flows Over Blunt Cones", *AIAA Paper No. 92-0324* (1992).

15) Mangler, W., "Zusammenhang zwischen Ebenen und Rotationssymmetrischen Grenzschichten in Kompressiblen Fluessigkeiten", *ZAMM 28*, 97-103 (1948).

16) Malik, M. R., and R. E. Spall, "On the Stability of Compressible Flow Past Axisymmetric Bodies", *J. Fluid Mech.*, Vol. 228, 443-463 (1991).

17) Marconi, F., M. Salas, and L. Yeager, "Development of a Computer Code for Calculating the Steady Super/Hypersonic Inviscid Flow Around Real Configurations: Volume I--Computational Technique", *NASA CR-2675* (1976).

18) Pruett, C. D., L. L. Ng, and G. Erlebacher, "On the Non-Uniqueness of the Parallel-Flow Approximation", *Proceedings of the ICASE/LaRC Workshop on Transition and Turbulence*, July 8 - August 2, 1991.

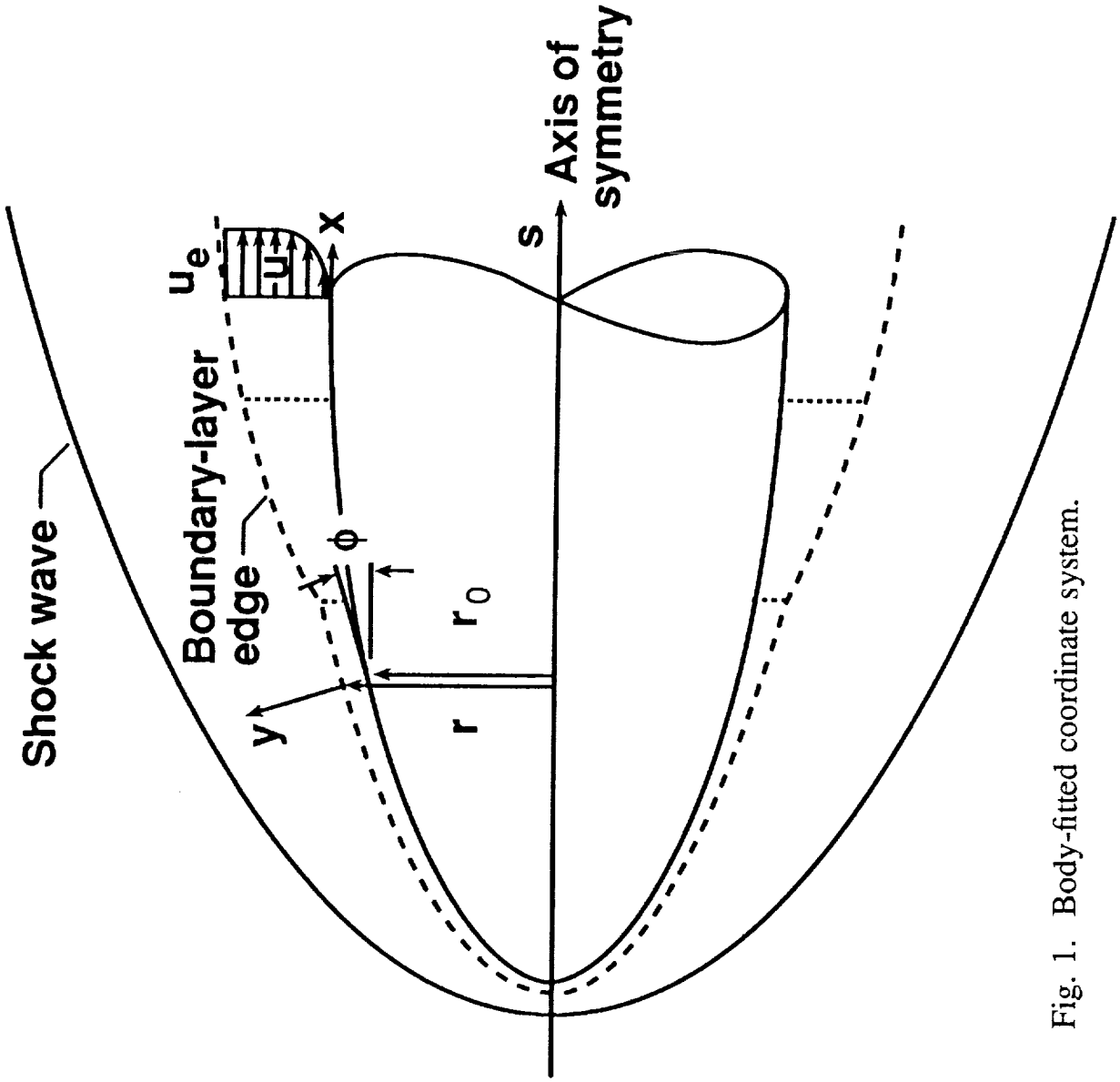

Fig. 1. Body-fitted coordinate system.

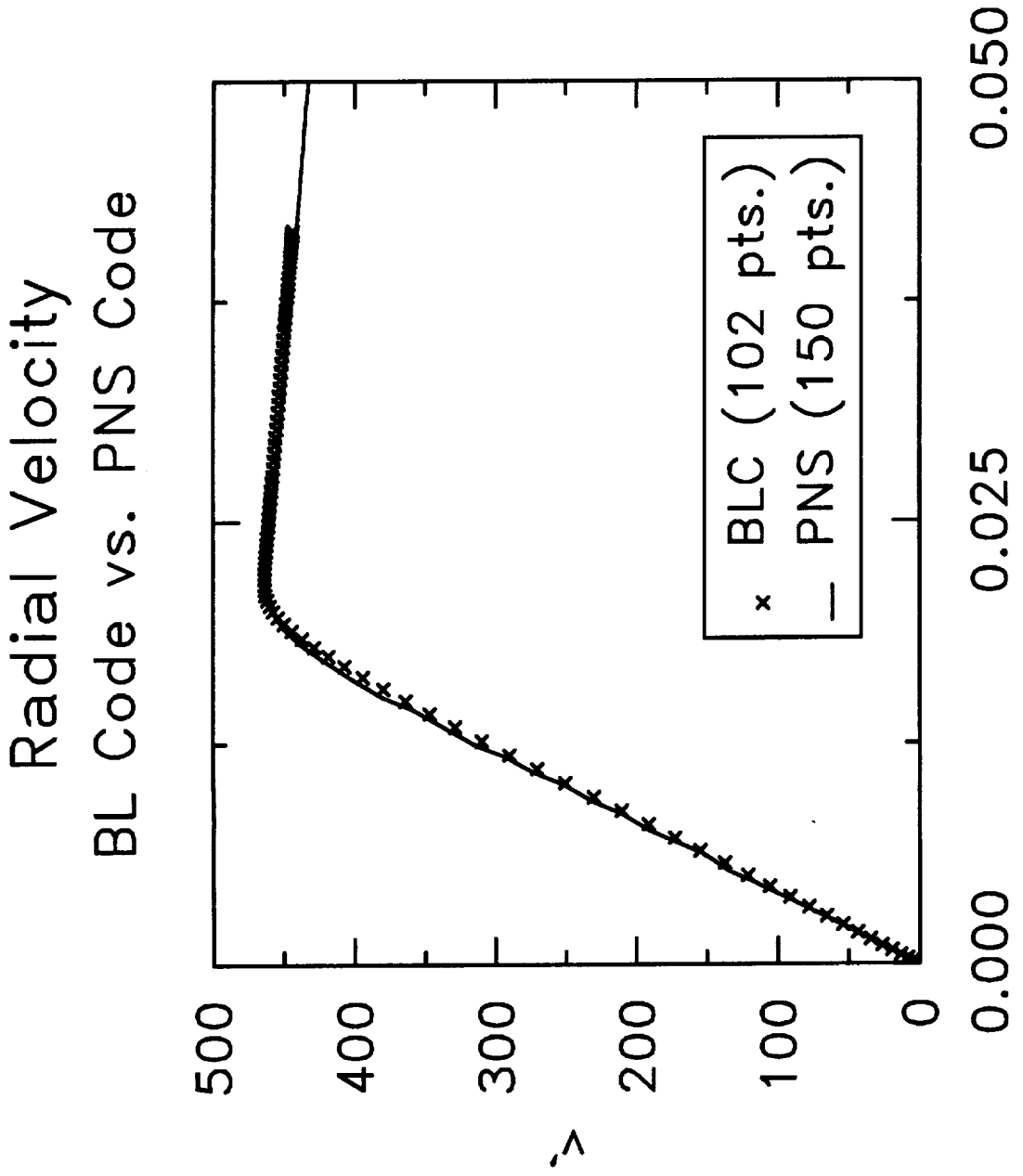

Fig. 2. Radial velocity at s^*=3.28 ft. (1 meter).

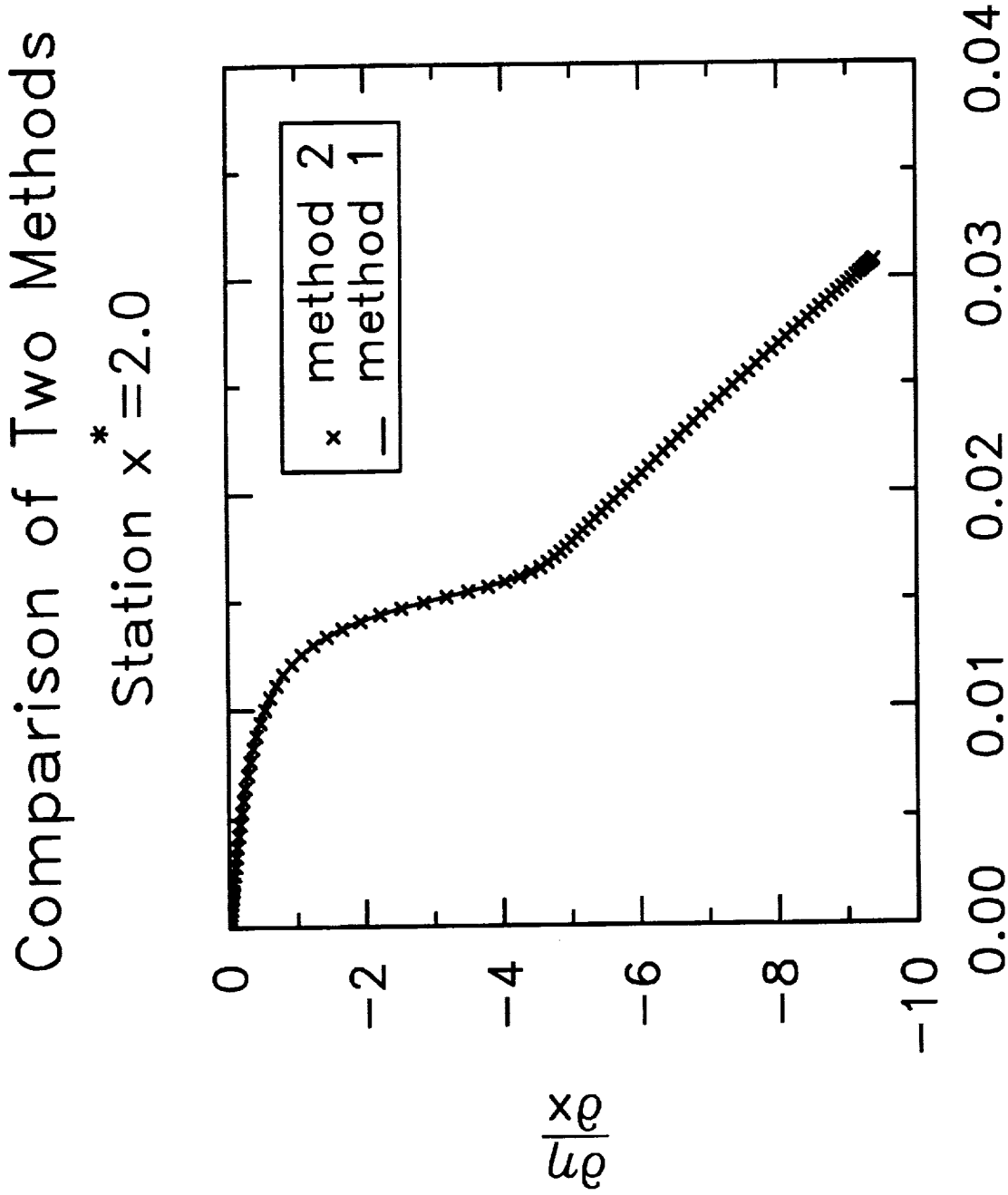

Fig. 3. Comparison of alternative derivations of $\frac{\partial \eta}{\partial x}$ at x^*=2.0 ft.

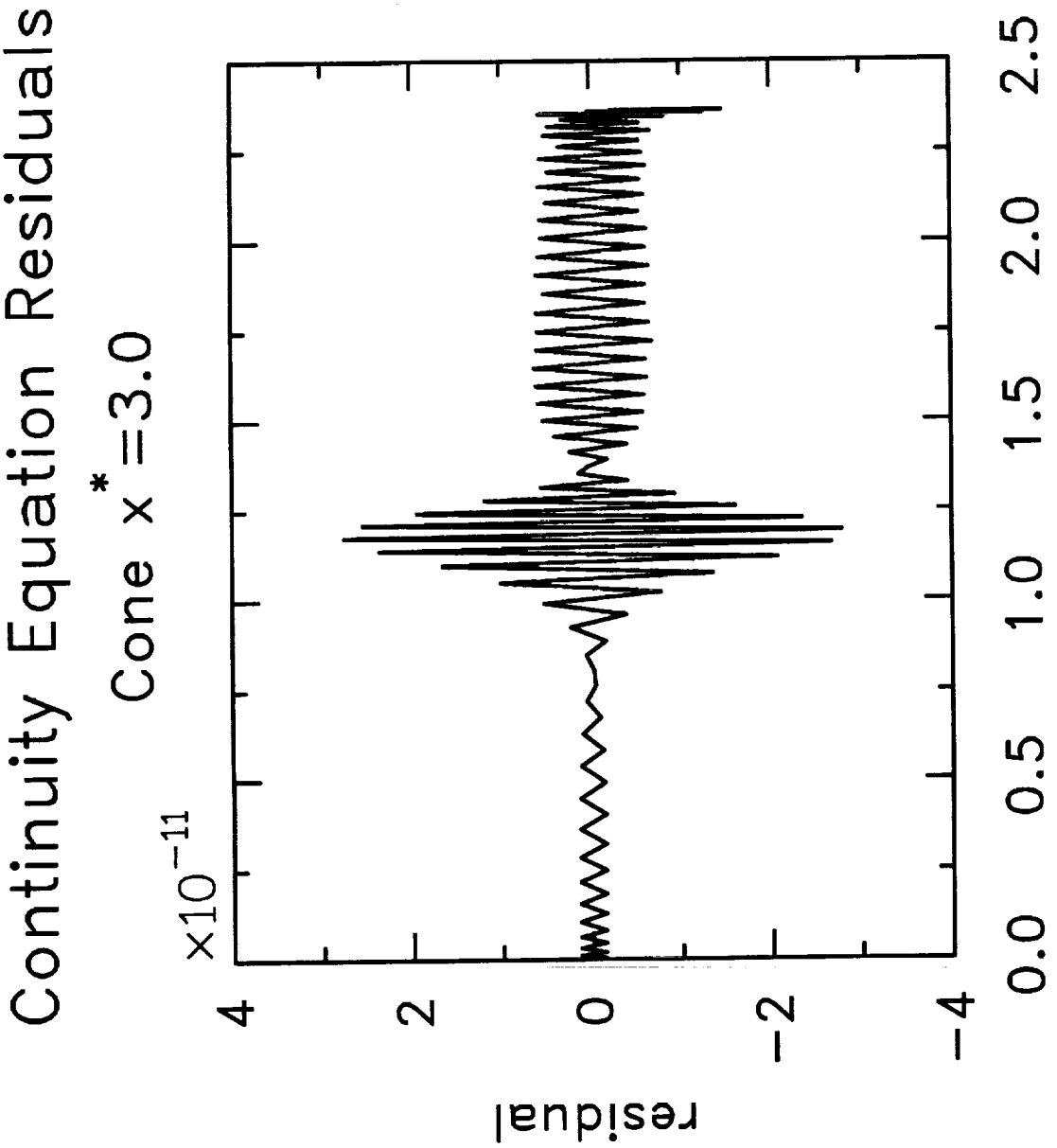

Fig. 4. Residual of the continuity equation.

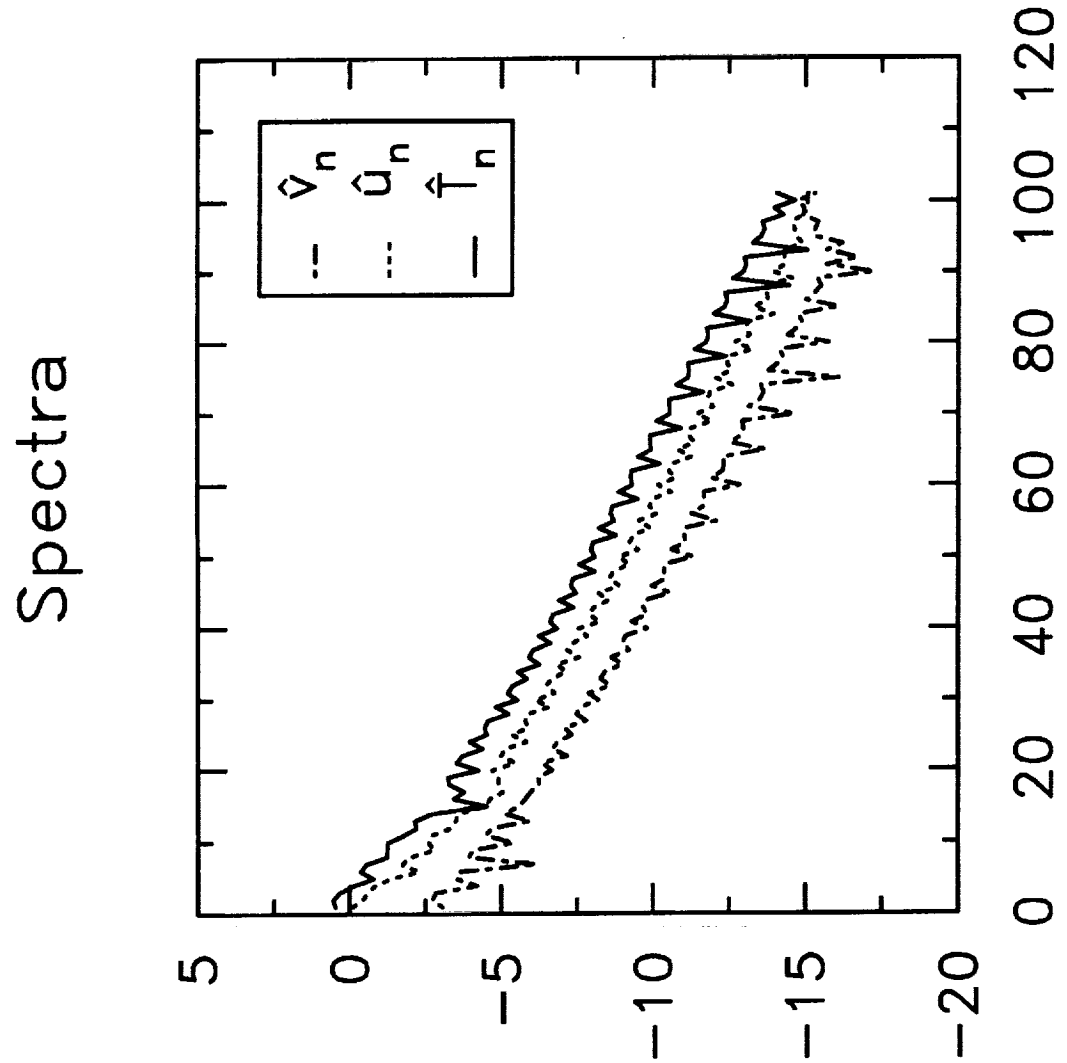

Fig. 5. Decay of the Chebyshev spectra.

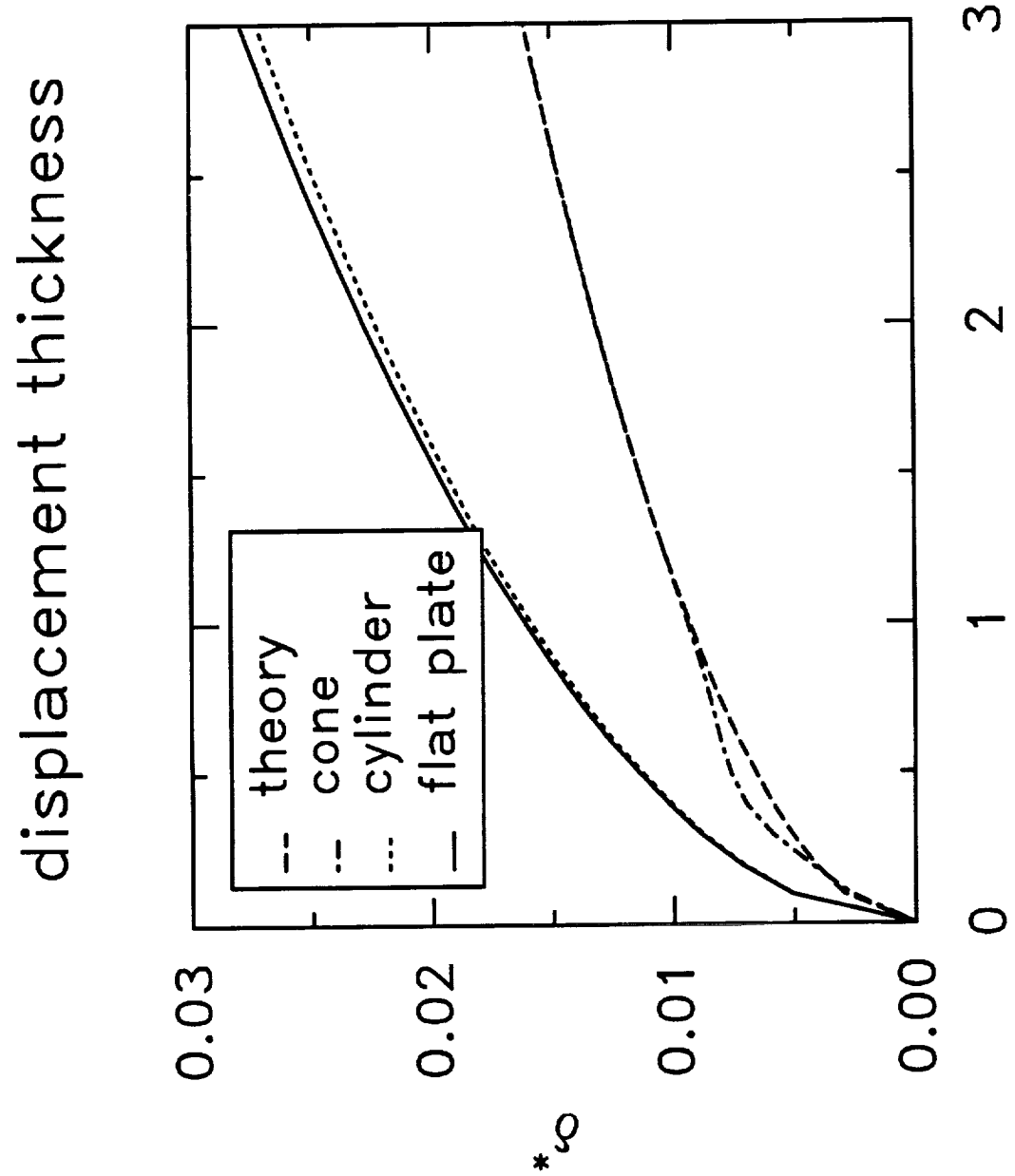

Fig. 6. Streamwise evolution of boundary-layer displacement thick ness.

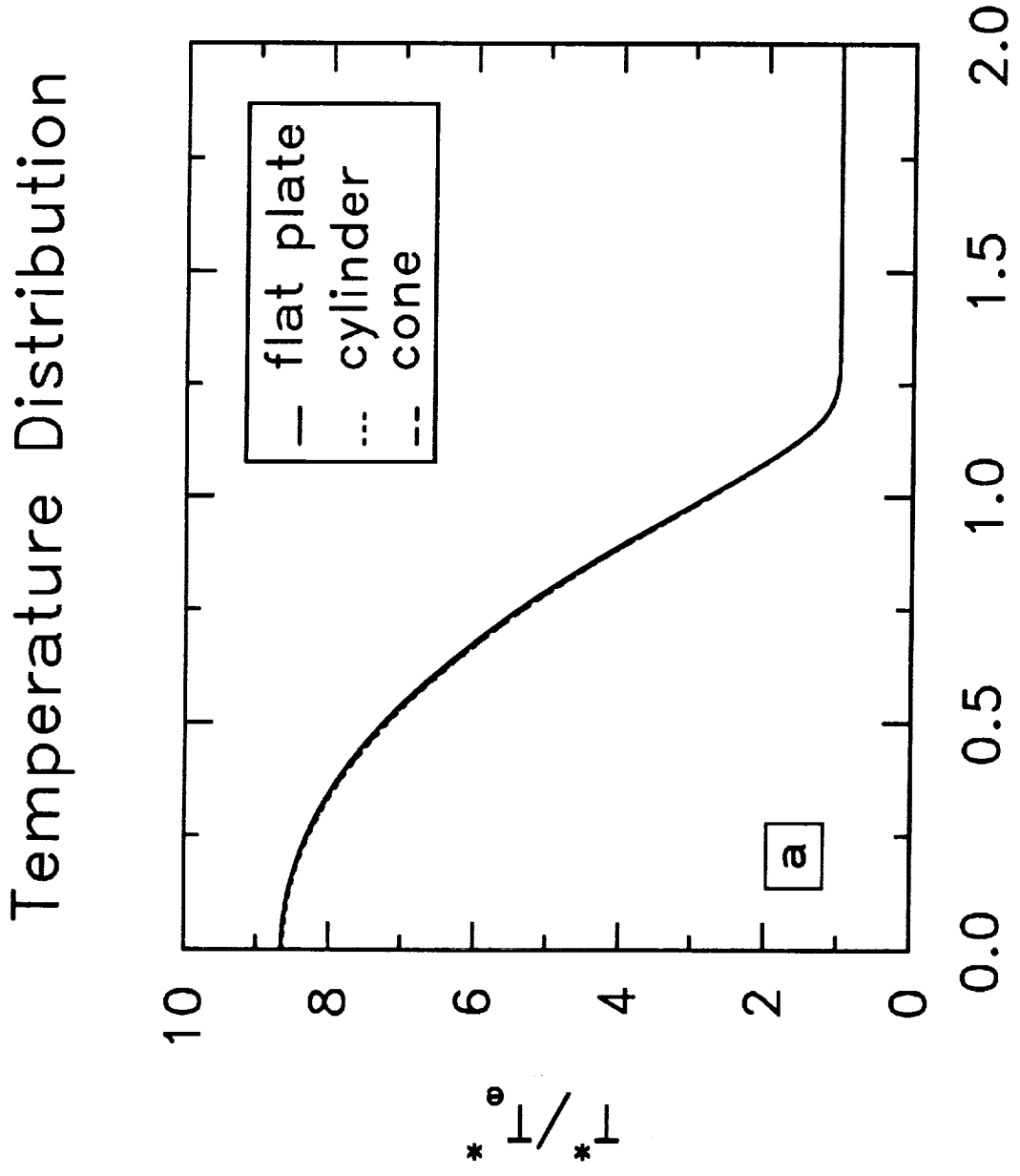

Fig. 7. Temperature a) streamwise velocity b) and wall-normal velocity c) distributions at x^*=3.0 ft.

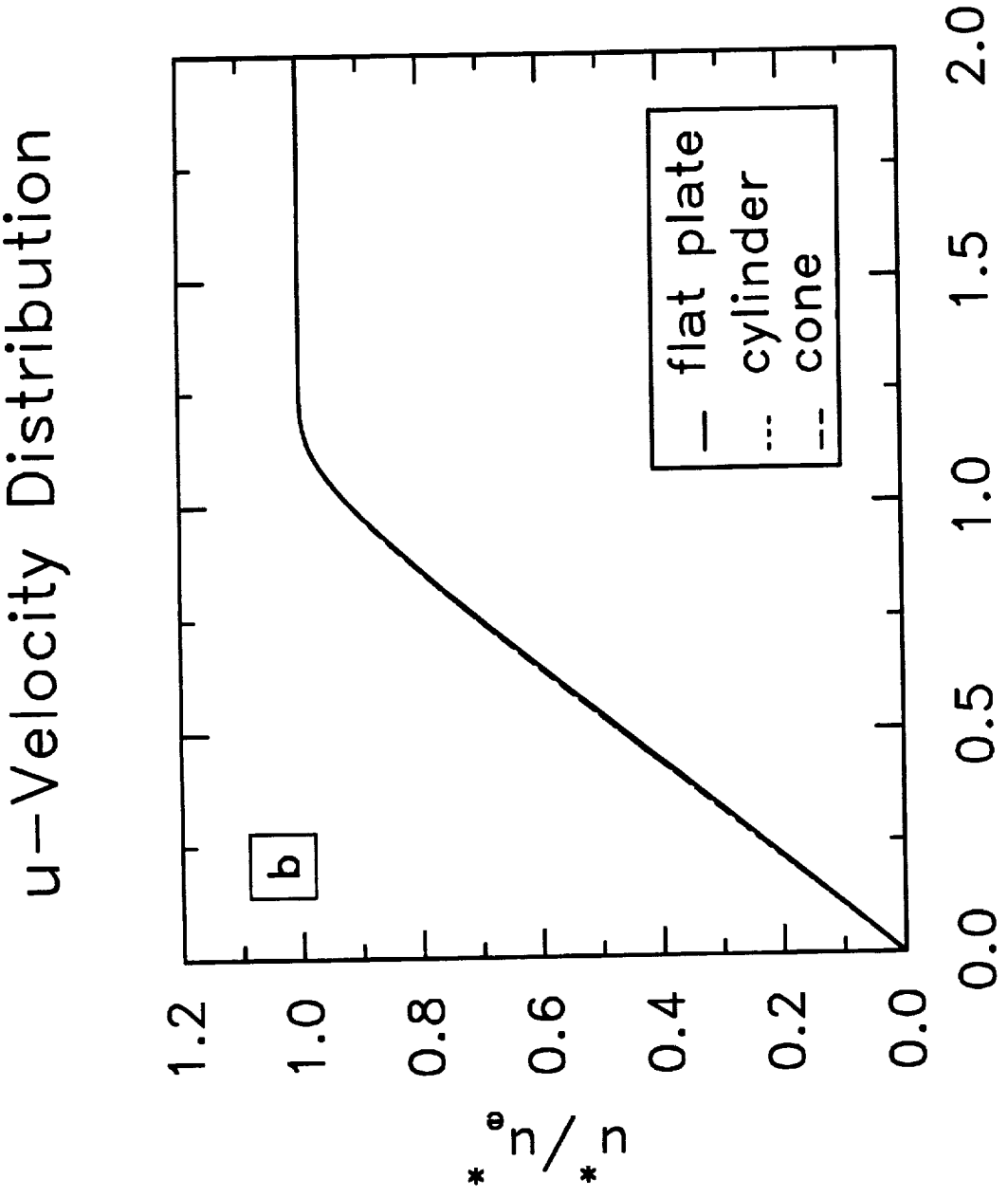

Fig. 7. Temperature a), streamwise velocity b) and wall-normal velocity c) distributions at $x^* = 3.0$ ft.

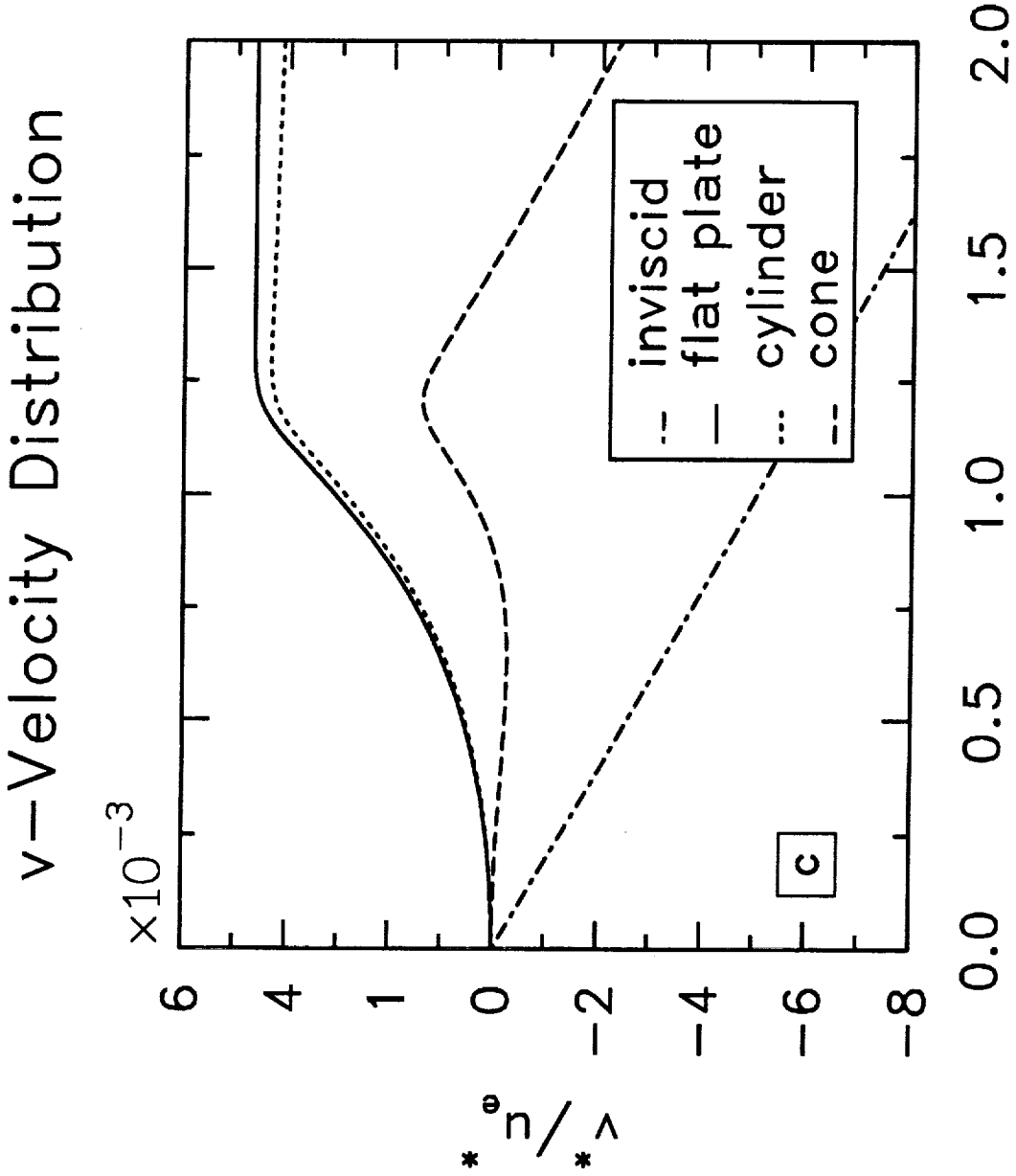

Fig. 7. Temperature a), streamwise velocity b) and wall-normal velocity c) distributions at $x^* = 3.0$ ft.

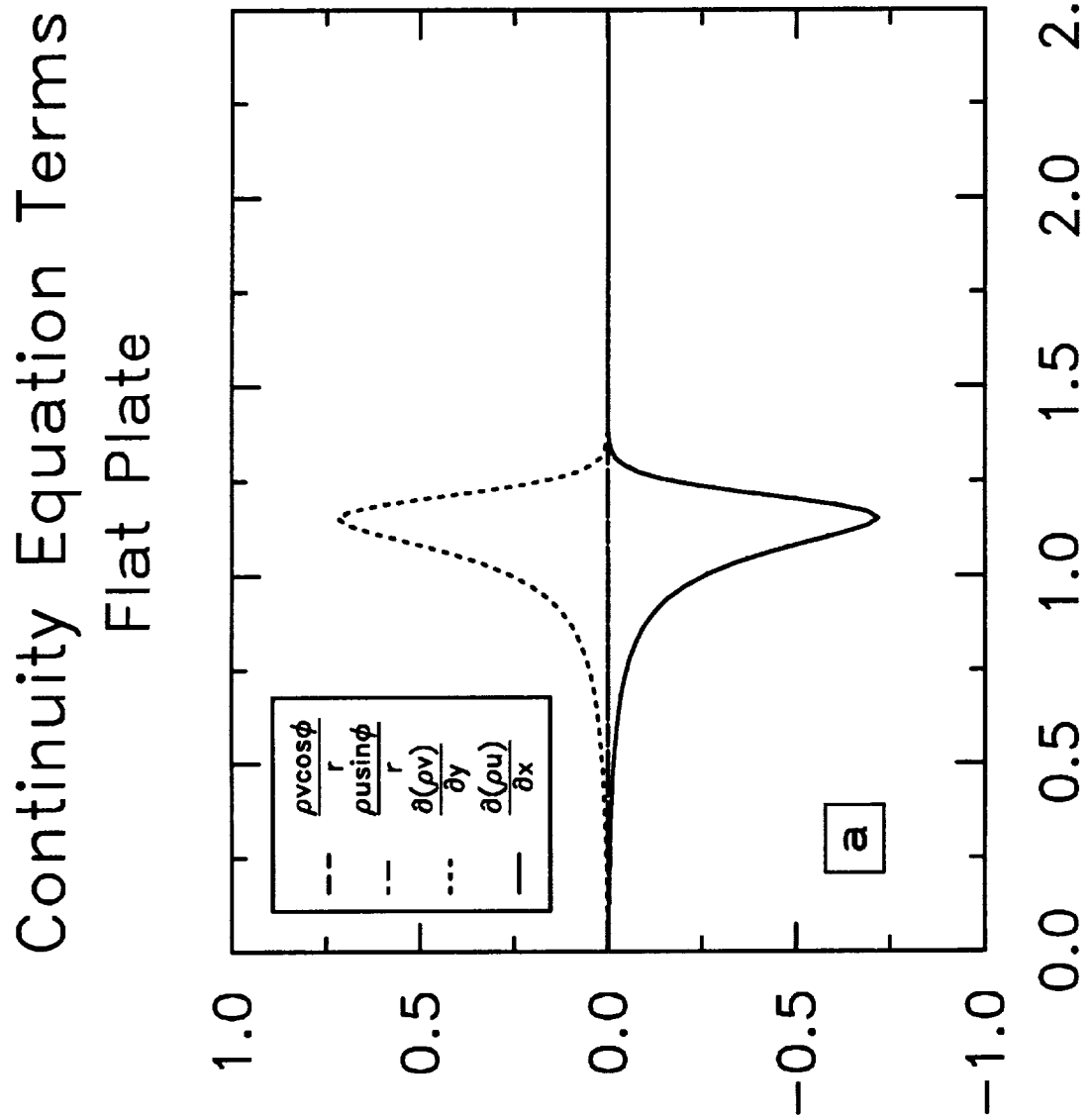

Fig. 8. Terms of the continuity equation compared at station x^*=3.0: a) flat plate; b) cylinder; c) cone.

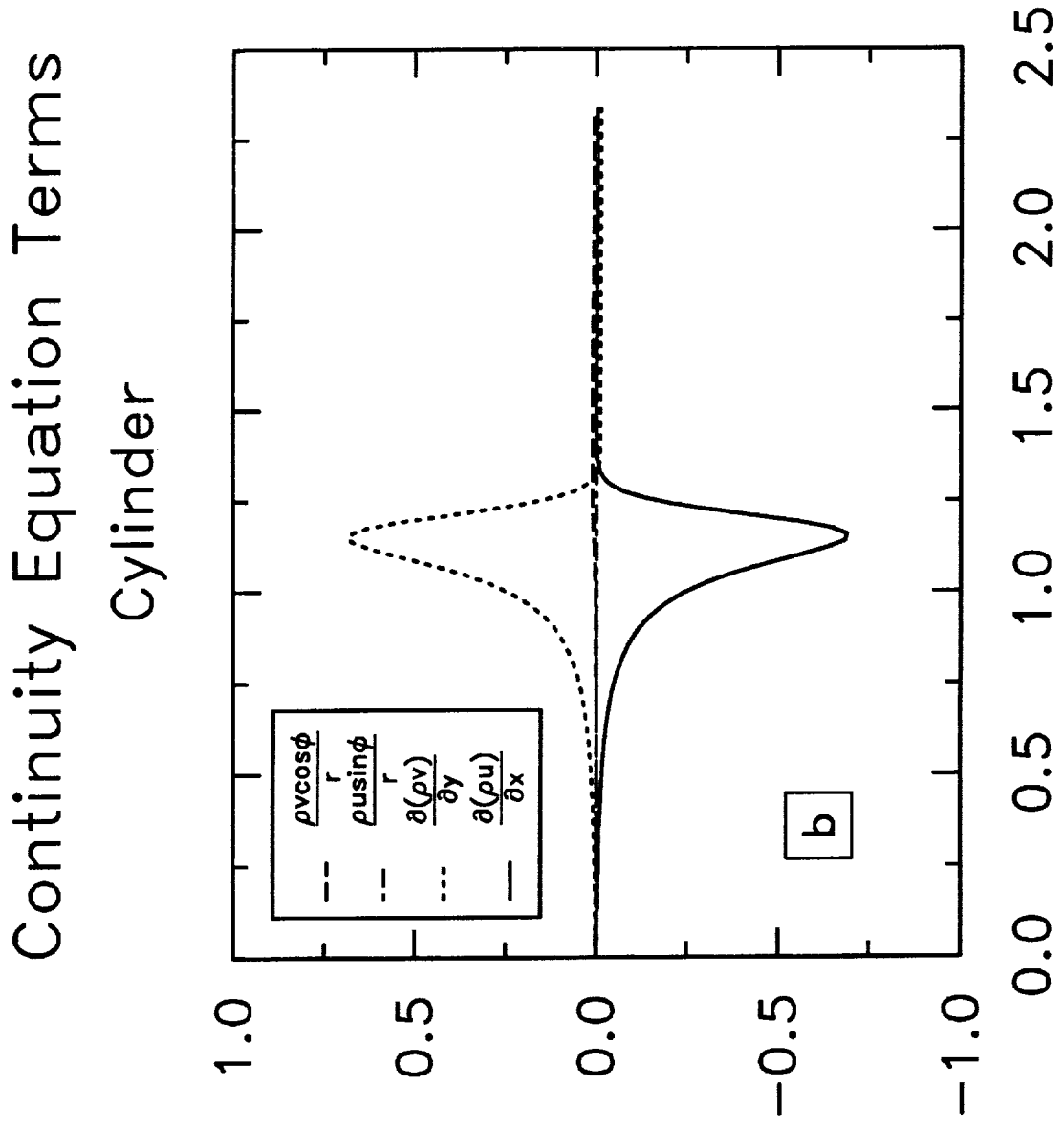

Fig. 8. Terms of the continuity equation compared at station x^*=3.0: a) flat plate; b) cylinder; c) cone.

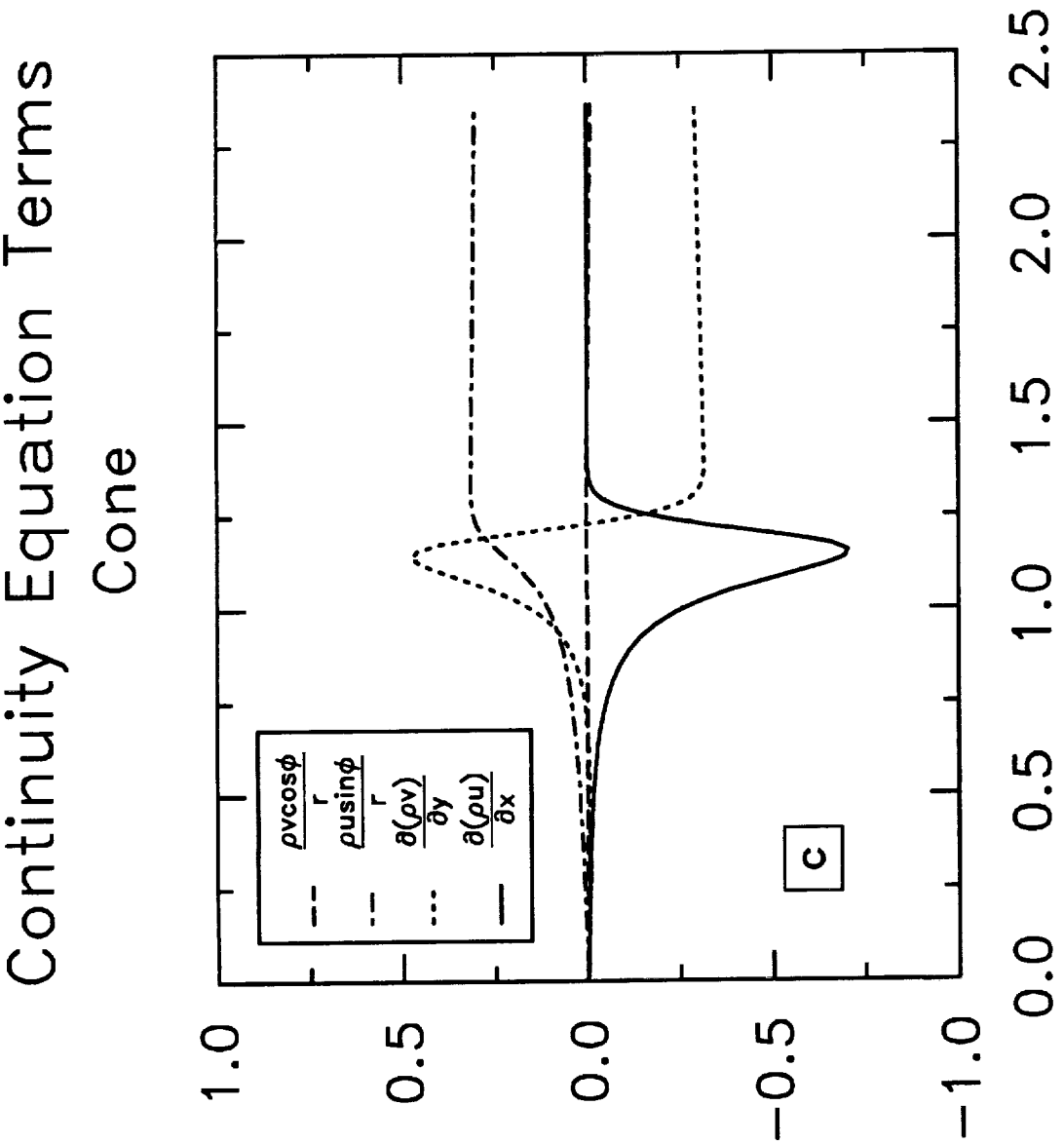

Fig. 8. Terms of the continuity equation compared at station x^* =3.0: a) flat plate; b) cylinder; c) cone.

REPORT DOCUMENTATION PAGE

Form Approved
OMB No. 0704-0188

1. AGENCY USE ONLY (Leave blank)	2. REPORT DATE	3. REPORT TYPE AND DATES COVERED
	December 1991	Contractor Report

4. TITLE AND SUBTITLE

On the Wall-Normal Velocity of the Compressible Boundary-Layer Equations

5. FUNDING NUMBERS

C NAS1-18599

WU 505-59-53-02

6. AUTHOR(S)

C. David Pruett

7. PERFORMING ORGANIZATION NAME(S) AND ADDRESS(ES)

Analytical Services and Materials, Inc.
107 Research Drive
Hampton, VA 23666

8. PERFORMING ORGANIZATION REPORT NUMBER

9. SPONSORING / MONITORING AGENCY NAME(S) AND ADDRESS(ES)

National Aeronautics and Space Administration
Langley Research Center
Hampton, VA 23665-5225

10. SPONSORING / MONITORING AGENCY REPORT NUMBER

NASA CR-4419

11. SUPPLEMENTARY NOTES

Langley Technical Monitor: James C. Townsend

12a. DISTRIBUTION / AVAILABILITY STATEMENT

Unclassified-Unlimited

Subject Category: 02

12b. DISTRIBUTION CODE

13. ABSTRACT *(Maximum 200 words)*

Numerical methods for the compressible boundary-layer equations are facilitated by transformation from the physical (x,y) plane to a computational (ξ,η) plane in which the evolution of the flow is "slow" in the time-like ξ direction. The commonly used Levy-Lees transformation results in a computationally well-behaved problem for a wide class of non-similar boundary-layer flows, but it complicates interpretation of the solution in physical space. Specifically, the transformation is inherently nonlinear, and the physical wall-normal velocity is transformed out of the problem and is not readily recovered. In light of recent research which shows mean-flow non-parallelism to significantly influence the stability of high-speed compressible flows, the contribution of the wall-normal velocity in the analysis of stability should not be routinely neglected. Conventional methods extract the wall-normal velocity in physical space from the continuity equation, using finite-difference techniques and interpolation procedures. The present spectrally-accurate method extracts the wall-normal velocity directly from the transformation itself, without interpolation, leaving the continuity equation free as a check on the quality of the solution. The present method for recovering wall-normal velocity, when used in conjunction with a highly-accurate spectral collocation method for solving the compressible boundary-layer equations, results in a discrete solution which is extraordinarily smooth and accurate, and which satisfies the continuity equation nearly to machine precision. These qualities make the method well suited to the computation of the non-parallel mean flows needed by spatial direct numerical simulations (DNS) and parabolized stability equation (PSE) approaches to the analysis of stability.

14. SUBJECT TERMS	15. NUMBER OF PAGES
Boundary-layer equations; compressible flow; spectral-collocation methods; wall-normal velocity; stability theory	40
	16. PRICE CODE: A03

17. SECURITY CLASSIFICATION OF REPORT	18. SECURITY CLASSIFICATION OF THIS PAGE	19. SECURITY CLASSIFICATION OF ABSTRACT	20. LIMITATION OF ABSTRACT
Unclassified	Unclassified	Unclassified	

NSN 7540-01-280-5500

Standard Form 298 (Rev 2-89)
Prescribed by ANSI Std Z39-18
298-102

NASA-Langley, 1991